Examination of the Relationship between Outgoing Infrared Window and Total Longwave Fluxes Using Satellite Data

PATRICK MINNIS

Atmospheric Sciences Division, NASA Langley Research Center, Hampton, Virginia

DAVID F. YOUNG

Lockheed Engineering and Sciences Company, Hampton, Virginia

EDWIN F. HARRISON

Atmospheric Sciences Division, NASA Langley Research Center, Hampton, Virginia

(Manuscript received 6 August 1990, in final form 5 March 1991)

ABSTRACT

The relationship between narrowband and broadband thermal radiances is explored to determine the accuracy of outgoing longwave radiation derived from narrowband data. Infrared window (10.2–12.2 μm) data from the Geostationary Operational Environmental Satellite (GOES) are correlated with longwave (5.0–50.0 μm) data from the Earth Radiation Budget Experiment (ERBE). A simple quadratic fit between the narrowband and longwave fluxes results in standard errors of 4.4%–5.3% for data that are matched closely in time and space. The use of matched regional flux data with temporal differences up to 59 minutes yields standard errors of 4.1%–5.4%. About 30% of the error may be attributed to limb darkening and spatial and temporal differences in the matched fluxes. The relationship shows a statistically significant dependence on the relative humidity of the atmosphere above the radiating surface. Although this dependency accounts for only about 1% of the standard error, it reduces the monthly mean regional errors by more than 10%. Data taken over land produced a relationship slightly different from data taken over water. The differences appear to be primarily due to daytime heating of the land surface. Cloud amount and cloud-top height also influence the narrowband–broadband relationship. Inclusion of these statistically relevant parameters does not affect the standard errors, but it reduces the monthly mean regional errors by 9%. Better humidity and temperature data and knowledge of cloud microphysics may be required to further improve the relationship. Using the best global fits, it is concluded that the monthly mean outgoing flux may be determined with an rms uncertainty of 1.7% using a single infrared window channel with coincident cloud and humidity data. The atmospheric structure that dictates the infrared–longwave relationship does not vary randomly; it changes with climate regimes. Thus, the errors resulting from using the global fits tend to be biases concentrated in certain geographical areas. This areal biasing dampens the utility of the narrowband data for monitoring the climatic-scale changes in the longwave flux. Regressions performed on a region-by-region basis eliminate most of the monthly mean regional bias errors. Thus, the regional regressions may be useful for short-term studies requiring high temporal sampling. Because of varying atmospheric conditions, regional regressions require continual calibration with broadband instruments, thereby limiting their utility for longer-term climate applications.

1. Introduction

Since the early 1970s, radiance measurements taken from narrowband instruments on operational meteorological satellites have been used to monitor components of the earth's radiation budget. Specifically, intensities in the visible (0.55–0.75 μm) and infrared window (10.2–12.2 μm) spectral intervals have been used as surrogates for shortwave (0.2–5.0 μm) and longwave (5.0–50.0 μm) radiances, respectively. Usually, the narrowband radiance is converted to broadband radiance or flux, either explicitly or implicitly, with a theoretical or empirical function. Infrared window radiances from the TIROS and NOAA satellites were converted into outgoing longwave fluxes using a single regression function to effect the narrowband-to-broadband conversion (e.g., Gruber and Winston 1978; Ohring et al. 1984). Ellingson et al. (1989a) have recently derived a theoretical update to those earlier formulas. Minnis and Harrison (1984b) developed separate conversion functions for land and ocean scenes for use with geostationary satellite data. Generally, the estimates of the rms errors in the longwave flux derived from these regression functions range from 7 to 11

Corresponding author address: Dr. Patrick Minnis, Atmospheric Sciences Division, NASA, Langley Research Center, Hampton, VA 23665-5225.

W m^{-2}. Use of these relationships implicitly assumes that the errors are random and, therefore, will be minimized by averaging the measurements over some period such as one month. The surface and atmospheric characteristics that give rise to the uncertainties, however, may not vary randomly over a given location. Over regions with average atmospheric or surface properties that differ significantly from the means implied in the regression functions, the rms errors will tend to become bias errors. Thus, while the operational data provide a long period of record of radiation-field variations, their use may result in significant errors and misinterpretation of the changes in the observed radiation fields.

Narrowband data from operational satellites are potentially valuable sources for validation of experimental satellite data results. The Earth Radiation Budget Experiment (ERBE; Barkstrom 1984) is a multisatellite project that is measuring the broadband components of the earth's radiation balance. One of the satellites, the Earth Radiation Budget Satellite (ERBS), is in a 57° inclined orbit, which allows the satellite to precess through all hours of the day over a given location during a period of approximately 36 days. This precession permits measurement of the complete diurnal cycle of radiation over that same time period. Combined with measurements of the ERBE instruments on the Sun-synchronous NOAA-9 (1430 LT equatorial crossing time), ERBE can provide more precise estimates of regional radiation budgets and better definition of the diurnal variation of outgoing broadband radiation than was heretofore possible (e.g., Harrison et al. 1983; Brooks and Minnis 1984). One means of determining how precisely the ERBE is accounting for spatial and temporal variations in the regional radiation fields and how precisely it is estimating the diurnal variations of the radiation budget is to compare its results with data taken at higher temporal and spatial resolutions. The Geostationary Operational Environmental Satellite (GOES) measures narrowband radiances every half hour at a resolution of ~7 km. It views a large portion of the western hemisphere, observing many different climate regimes. To be useful as a quantitative validation source, the narrowband GOES data must be converted to broadband fluxes. The accuracy of that conversion process, however, must be smaller than the errors due to sampling by the ERBE. The magnitudes of the conversion errors noted above are too large for the narrowband data to be directly useful for validation of the ERBE time–space averaging errors.

Instead of converting GOES radiances to broadband fluxes, this paper compares narrowband, infrared window (IR) GOES data, as is, with broadband longwave (LW) data from ERBE. The comparison also considers how surface type and atmospheric components, specifically temperature, water vapor, and cloud height, influence the narrowband–broadband relationship. Narrowband radiances from GOES and LW radiances and fluxes from the ERBS taken during April 1985 are the primary data source used to explore the IR–LW relationship. Radiation data taken by the *NOAA-9* Advanced Very High Resolution Radiometer (AVHRR) and ERBE scanning radiometer during October 1986 are also used to complement the GOES–ERBS results. The primary goal of this study is to improve our understanding of the GOES/ERBE relationship sufficiently to be able to use GOES data for validation of the time–space averaging results of ERBE (Brooks et al. 1986).

2. Data and methodology

Two approaches are considered here. The first approach follows that used by Minnis and Harrison (1984b), who matched the fields of view of two different satellites and performed regressions on the observed narrowband and broadband radiances. These data are referred to as ray-matched (RM) data. The second approach uses all flux data from the two satellites, which are taken within one-half hour of each other over a given region. These data are denoted as hour-box matched (HB). The former technique uses only those instantaneous irradiances that are cotemporal, collocated, and coangled to relatively strict tolerances. Thus, the ray-matching technique minimizes the effects of space and time mismatching, while the hour-box–matching method, which use regionally averaged fluxes, maximizes both temporal and spatial sampling. The domain covers the areas between 50°N and 50°S latitudes and 55° to 155°W longitudes. Only data between 1 and 21 April 1985 are used since the GOES IR channel suffered a sudden calibration shift around 22 April. For the HB regressions, the domain is divided into 1600 (2.5° × 2.5°) regions.

a. Satellite data

Narrowband data are taken hourly beginning on the UTC (Universal Coordinated Time) hour at a nominal resolution of 6.9 km, hereafter referred to as 7 km, from the *GOES-6* located over the equator at ~108°W. Characteristics of the GOES IR channel are given by Montgomery and Uccellini (1985) and WCRP (1987). Calibration of the instrument accounts for the response function of the IR filter (Menzel 1980). The IR data are recorded as equivalent blackbody temperatures, T. These data are converted to narrowband radiances using

$$L_n = B(T),$$

where B is the Planck function evaluated at 11.5 μm. The radiances are adjusted to the nadir view by

$$L_n(0°) = \gamma_n L_n(\theta),$$

where the limb-darkening function is

$$\gamma_n = 1, \quad \text{if} \quad \theta < 11°, \quad \text{else}$$

$$\gamma_n = 1.00067 + 0.03247 \ln(\cos\theta). \quad (1)$$

This formula approximates the IR limb-darkening function used by Minnis and Harrison (1984a), where θ is the viewing zenith angle. The narrowband flux is

$$M_n = 2L_n(0°)\int_0^{2\pi}\int_0^{\pi/2}\gamma_n \sin\theta\cos\theta d\theta$$

$$= 6.18L_n(0°), \quad (2)$$

where the factor two (in microns) is used here to account for the bandwidth of the GOES sensor. Its use assumes a flat sensor response.

Broadband radiances, L_b, taken with the ERBS scanner have a nominal nadir footprint of $\sim 31 \times 47$ km^2. Each measured radiance is classified as clear, partly cloudy, mostly cloudy, or overcast and converted to flux, M_b, by multiplying by π and an anisotropic factor, which accounts for limb darkening (Smith et al. 1986). The fluxes for all classifications are averaged together for a given region and satellite overpass to obtain a single value of M_b for the region. For ease of processing, the measurement times assigned to the ERBE fluxes are adjusted to the nearest half hour of local time (Brooks et al. 1986).

Ray-matched data are correlated if they are taken within ten minutes of each other over the same location with differences of less than 8° and 10° in their respective viewing zenith and relative azimuth angles. The viewing angle constraints are expected to introduce larger uncertainties at high viewing zenith angles due to an increasing rate of change of limb darkening with θ. Such increased uncertainty should be minimized, however, since both IR and LW radiances are converted to fluxes with their respective limb-darkening functions. A narrowband radiance for an equivalent ERBS field of view (FOV) is obtained by computing the average of all GOES radiances located within the ERBS FOV, which is assumed to be equivalent to a 4 $\times$ 4 array of GOES pixels. The mean radiances are converted to irradiance using (2) and paired with the corresponding ERBS fluxes, then used in the RM correlations described below. The HB data were created by matching a GOES-derived regional IR flux, which was taken within 59 minutes of the corresponding ERBS regional LW flux.

Cloud parameters were also derived for each region. The hourly, regional GOES IR data, together with the collocated 7-km visible radiances, were analyzed with the methodology of Minnis et al. (1987) to obtain cloud amounts, heights, and temperatures.

The AVHRR data taken from the Global Area Coverage (GAC) dataset have a nominal resolution of ~4 km. To match the GOES IR channel, the equivalent blackbody temperatures from the NOAA-9 AVHRR channels 4 (10.0–11.6 μm) and 5 (11.3–12.5 μm) were averaged to obtain a single IR temperature for each AVHRR GAC pixel. The AVHRR is a cross-track scanner like the ERBE radiometer. Thus, the *NOAA-9* ERBE and AVHRR data are matched much more closely in time and space than the GOES and ERBS data. Matching of the ERBE and AVHRR fields of view is described later.

b. Humidity data

Temperature and moisture data taken from the 12-hourly NMC (National Meteorological Center) gridded analyses are used to compute the column relative humidity, r, for each pair of flux or radiance data. This column relative humidity is defined as the mean relative humidity between the GOES level and 300 mb. The GOES level is defined as the pressure height from the NMC vertical profile that corresponds to the equivalent blackbody temperature of L_n or M_n. The NMC profiles are interpolated to the UTC hour closest to the time of the matched data.

c. Conceptual model

The flux or radiance measured by the satellite is composed of emissions and reflections from the atmosphere and from the surface, which is considered here to be some combination of ocean, land, and clouds. In a greatly simplified form, the flux may be expressed as

$$M = (1 - \epsilon_a)\epsilon_s f(T_s) + \epsilon_a f(T_a), \quad (3)$$

where ϵ_s and ϵ_a are the effective surface and atmospheric emissivities, T_s is the surface temperature, and T_a is the effective temperature of the atmosphere. The function $f(T)$ refers to either the Planck function integrated over the IR interval or the Stefan-Boltzmann law for the LW. The peak of the Planck function ranges from 14.5 μm at 200 K to 8.9 μm at 325 K with maxima at 237 K and 283 K for 12.2 μm and 10.2 μm, respectively. This model assumes a nonreflecting surface and neglects any near-surface discontinuities. For the IR flux, atmospheric emissivity is due mostly to emission in the water vapor continuum. This emission depends primarily on the vertical structure of temperature and saturation vapor pressure. The LW atmospheric emissivity depends on the water vapor continuum, numerous water vapor absorption lines, and the absorption lines of other gases such as ozone and carbon dioxide. The surface emissivity is virtually independent of wavelength for some surfaces, such as forests and water, but not for others, such as deserts (Prabhakara and Dalu 1976). Cloud emissivity also exhibits some spectral dependency (Ackerman and Smith 1990), which would affect the IR–LW relationship. Finally, the effective atmospheric temperature depends on the vertical temperature profile and distribution and total mass of absorbers above the radiating surface.

d. Regression analyses

The basic form used here for empirically relating the narrowband and broadband irradiances is

$$M_b = a_0 + a_1 M_n + a_2 M_n^2, \quad (4)$$

where a_i are the regression coefficients (e.g., Minnis and Harrison 1984b). Over the range of terrestrial temperatures (i.e., ~190 to 340 K), the blackbody flux at 11.5 μm is essentially linear with the total blackbody irradiance for the same temperature. At extremely low temperatures, the contribution of the IR spectral interval to the total blackbody irradiance asymptotically approaches zero while the LW flux remains substantially greater than zero. Thus, the form of (4), which does not permit this asymptotic behavior, should only be applied over the range of meteorological temperatures. The squared term in (4) is used to account for the absorption and emission of gases in the atmosphere. These effects depend on pressure, temperature, species concentration, and wavelength so that the *effective* IR blackbody irradiance will not necessarily vary linearly with the *effective* LW blackbody irradiance emanating from the earth–atmosphere system.

The data were regressed on (4) for land and ocean separately using a least-squares technique. Correlations using these broad categories are referred to as global fits. Because of storage limitations, the regression analyses were limited to a maximum of 6000 data points. Regular sampling of the HB data stream was used to accommodate that limit for larger datasets. Sampling for the RM dataset depends on the occurrence of coincident viewing conditions which, if they occur, are limited to a few narrow swaths on any given ERBS orbit. All pixels in this swath are used in the regression so that in homogeneous areas, there is redundant sampling of the particular set of conditions. The ERBS is in a precessing orbit, however, so that the sampled regions vary from day to day. Although some situations may not be sampled over the course of 21 days, the range of sampled conditions should be sufficient to obtain a reasonable regression fit for mean conditions. Sampling of the HB data is more complete. There are approximately 50 matches between the ERBS and GOES regional averages for each region during the sampling period. The HB data were arranged first by region, then in chronological order for each region. The periodic sampling applied to this ordered dataset results in nearly uniform geographical sampling and quasi-random temporal sampling.

3. Results and discussion

a. Global quadratic fits

A scatterplot for the ocean RM data and the resultant fit to (4) are given in Fig. 1a. The HB fluxes from ocean regions are shown with their fit in Fig. 1b. The fits to the data taken over land are very similar except that M_b computed for a given value of M_n is about 2.5 W m^{-2} lower, on average, than the corresponding ocean broadband irradiances. Statistics and coefficients describing these regression curves are summarized in Table 1. Both types of fits produce similar statistics. Almost 91% of the variance is explained with the quadratic fits over the ocean, while approximately 88% is explained over land. The RM and HB root-mean-square errors (RE) are similar with lower values over ocean than land. The primary differences between the RM and HB results are seen in the coefficients. Uncertainties in the coefficients, as reflected in the standard errors (SE) of the coefficients, are greater for the

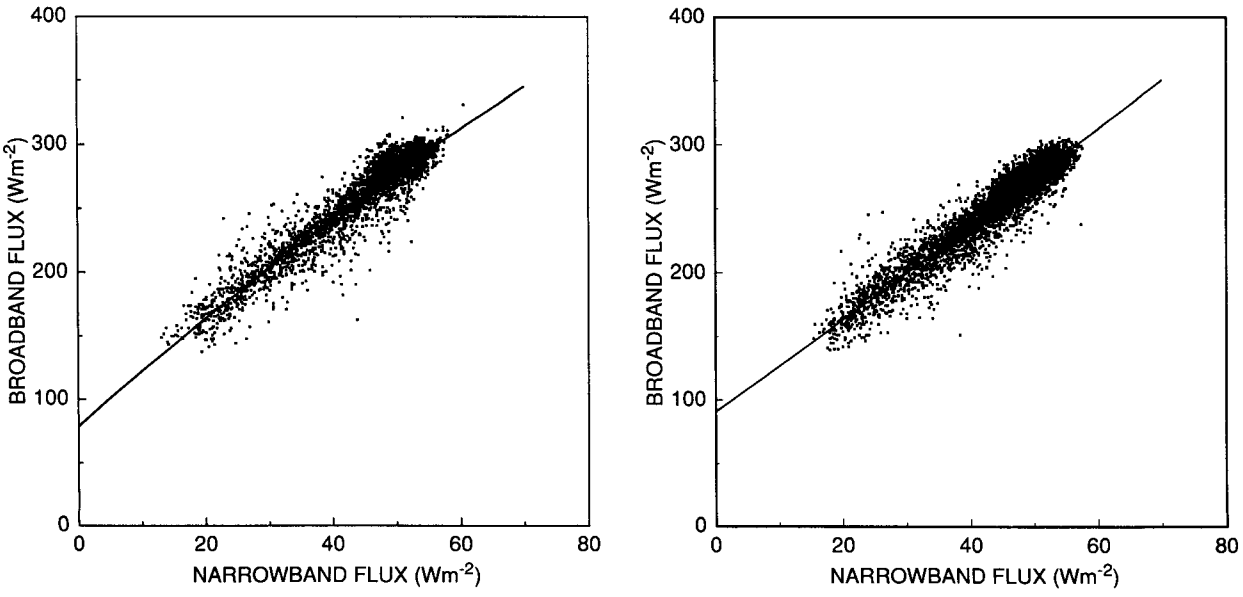

FIG. 1. Correlations using (4) for (a) ocean RM radiance data and (b) ocean HB flux data.

TABLE 1. Coefficients and statistics of radiance and flux fits to Eq. (4).

Background	a_0 (W m^{-2})	a_1	a_2 (W^{-1} m^2)	R^2	RE [% (W m^{-2})]	Samples
			RM data			
Ocean	78.75	4.416	−0.0085	0.904	4.4 (11.3)	4344
SE of coefficient (%)	3.6	3.4	21.9			
Land	72.23	4.721	−0.0134	0.885	5.3 (12.9)	2054
SE of coefficient (%)	6.1	4.7	20.2			
			HB data			
Ocean	90.54	3.568	0.0021	0.910	4.1 (10.3)	6000
SE of coefficient (%)	0.7	3.4	72.0			
Land	77.64	4.397	−0.0111	0.881	5.4 (12.5)	5203
SE of coefficient (%)	0.8	2.7	13.5			

RM data than for the HB data. These uncertainties, discussed later, are probably due to a reduced sampling population and to field-of-view mismatching. The relatively large sizes of the coefficient SE and the small values of a_2 suggest that the squared term is unnecessary for the ocean fit. Use of the linear fit over the ocean explains as much variance as the quadratic fit. Application of stepwise regression analysis (e.g., Draper and Smith 1981) to the data confirm this conclusion; the partial F statistic for the quadratic term is 1.6, considerably less than the desired threshold for significance at the 95% confidence level. Over land, the squared term is more significant. Its magnitude is greater and its error is smaller for the HB data, and its partial F statistic is 54. Use of the quadratic, however, increases the amount of explained variance by only 0.2% over the linear regression. As seen later, the squared term is important for accounting for flux variations at high surface temperatures over land. If the uncertainties in the coefficients are considered, it may be concluded that there is no statistical difference between the land HB and RM results. Over ocean, the differences are significant.

Differences in the coefficient values lead to RM-based values of M_b that are 1.4% greater than the corresponding HB results over ocean for the observed range of IR fluxes, $15 < M_n < 55$ W m^{-2}. The RM land coefficients yield a similar overestimate of LW flux compared to the HB fit over the range $15 < M_n < 75$ W m^{-2}. Most of the differences are probably due to discrepancies between the atmospheric and surface conditions sampled in the two datasets. The fits based on the HB data cover a greater range of conditions. They are based on nearly 6000 data pairs selected in an essentially random fashion from a pool of almost 80 000 nearly independent samples. The RM regressions are based on much less sampling of data that, in many cases, are not statistically independent due to contiguity. As seen later, some of the sampling discrepancies may be eliminated by considering atmospheric conditions. Judged against the statistical measures of the RE and the squared correlation coefficient, there is no apparent advantage to performing the regressions with temporally and spatially matched data as executed with the RM dataset. Since there is better sampling obtained with the HB dataset, however, it is concluded that the HB coefficients are more representative of a global fit than the RM data.

Minnis and Harrison (1984b) performed an analysis identical to the RM regressions of this study, except that LW *radiances* from the *Nimbus-7* Earth Radiation Budget scanner were compared to IR *radiances* from the *GOES-2* satellite. The standard errors from their results are slightly greater than those found here. They found a slightly greater separation between the land and ocean fits than was determined from the HB data. Ohring et al. (1984) also performed an IR–LW regression using *Nimbus-7* radiances. They used IR data from the Temperature and Humidity Infrared Radiometer (THIR) on board the *Nimbus-7* satellite. The THIR IR window covered the spectral interval 10–12 μm. Since it operated simultaneously with the ERB, there was better spatial and temporal matching of the two datasets than was possible for the GOES and *Nimbus-7* satellites. The Ohring et al. (1984) regression was performed using all data without regard to surface type. That regression also used a quadratic fit, but there is no offset, the independent variable is T, and the dependent variable is the broadband flux equivalent temperature. The rms errors for the THIR regression fit are $\sim$11 W m^{-2}, nearly identical to the mean rms error in Table 1.

Figure 2 shows a comparison of the HB results with those from Minnis and Harrison (1984b) and from Ohring et al. (1984). The Minnis and Harrison (1984b) LW radiances were converted to flux using the factor of 2.95, the hemispherical integral of the *Nimbus-3* limb-darkening function used in their analysis. The IR radiances were converted to M_n with (2). Narrowband fluxes for the THIR fit were computed from the win-

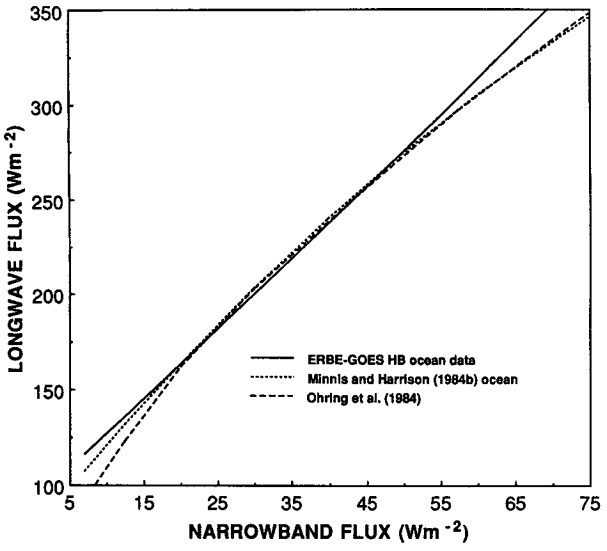

FIG. 2a. Comparison of empirical narrowband–broadband longwave formulas over ocean.

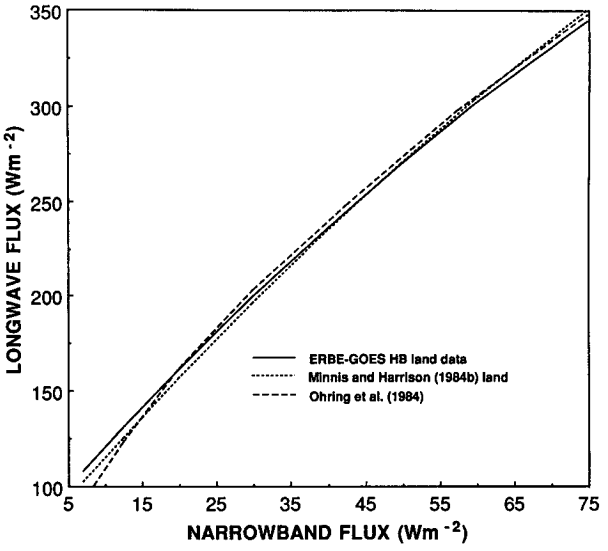

FIG. 2b. Comparison of empirical narrowband–broadband longwave formulas over land.

dow temperatures using the Planck function at 11.5 μm and equation (2). The corresponding values of M_b were taken from Fig. 3 of Ohring et al. (1984). The three curves over ocean (Fig. 2a) agree to within ± 2 W m^{-2} over the range of M_n from 20 to 55 W m^{-2}. The THIR fluxes are considerably lower than the other two results for the remainder of observed narrowband fluxes between 13 and 20 W m^{-2}. The reason for the differences at the lower end is not immediately apparent. Equation (4) fits the HB data well at the lower end. The range of observed IR temperatures for the Ohring et al. (1984) data is not known. Figure 2b shows less agreement between the two land fits and the THIR curve. Since the Ohring et al. (1984) curve matches the ocean results, it cannot match the land results from the other datasets. The Minnis and Harrison (1984b) curve is lower than the HB fit at lower temperatures and slightly greater at the highest temperatures with an rms difference of 3 W m^{-2} over the range of observed IR fluxes between 13 and 75 W m^{-2}. These differences may be due to spatial and temporal sampling inconsistencies. They are no greater than those found in the comparison of the HB and RM data over land, suggesting that there is no statistically significant difference between the HB and Minnis and Harrison (1984b) fits. Despite all of the potential differences (e.g., calibration, sampling, limb darkening, resolution, spectral filters) between the three datasets, there is surprisingly good agreement in the resulting relationships between IR and LW irradiances. Additional discussion of these differences is given later in this paper.

b. Effects of water vapor

Figure 3 shows the mean relative humidity above the GOES level for all of the HB data. Mean total cloud amount for all of the HB data is shown in Fig. 4. The low-humidity areas ($r < 30\%$) correspond to the subtropical anticyclones off the coasts of California and Chile and east of Puerto Rico. The clear belt at the equator (Fig. 4) is very humid according to these results. Other areas of relatively high humidity include the frontal cloud zone near 40°S, the Great Lakes, and the coast of Peru. Cloud cover is most extensive under the Pacific anticyclones, over the Amazon Basin, North Atlantic, and North Pacific.

Flux differences between the GOES global HB flux fits using (4) and the corresponding ERBE irradiances,

$$\Delta M = M_b(\text{GOES}) - M_b(\text{ERBE}),$$

were computed for each pair of HB data. These differences were then binned and averaged according to the value of r. The results shown in Fig. 5 with the corresponding standard deviations reveal an almost exponential variation of the difference with r. There is little effect on ΔM for relative humidities greater than 50%. At lower humidities, ΔM changes significantly with r such that the global regression fit substantially underestimates the LW flux in dry atmospheres. The typical value of the standard deviation in ΔM for a given r is around 10 W m^{-2} as indicated by the error bars shown in the figure. Since there are more than a thousand samples per bin, however, the standard error of the mean value in each bin is generally around 0.1 W m^{-2}, indicating the trend is significant.

Using Fig. 5 as a guide, the water vapor is included in the regression equation as follows:

$$M_b = a_0 + a_1 M_n + a_2 M_n^2 + a_3 M_n \ln r, \quad (5)$$

where the column relative humidity is given in percent. The HB data were reanalyzed with (5) yielding the

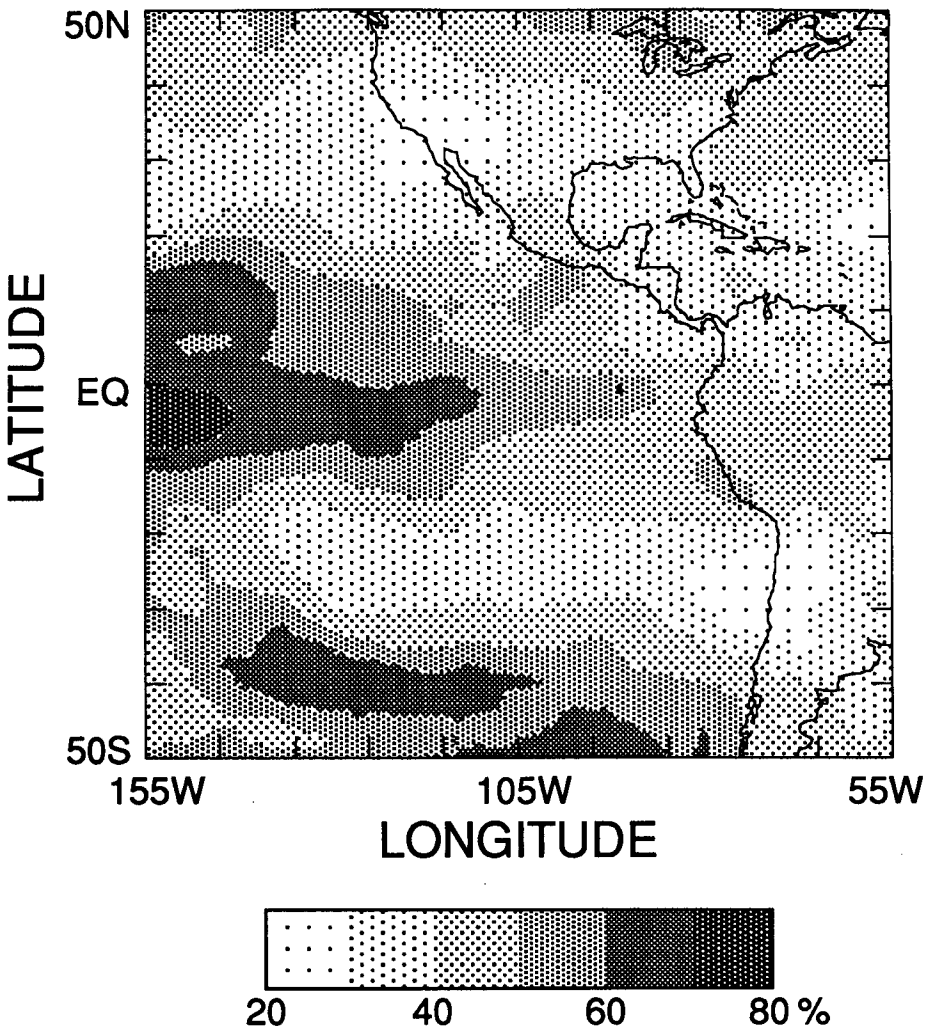

FIG. 3. Mean relative humidity in percent for HB data, 1–21 April 1985.

coefficients listed in Table 2. Figures 6a and 6b show the data and the resulting curves for relative humidities of 20%, 40%, 60%, and 80% over ocean and land, respectively. Over the range of r from 20% to 100%, the estimated broadband flux for a given narrowband flux varies by 3 W m^{-2} at T = 215 K up to 20 W m^{-2} at T = 305 K.

The RM data were also fitted with (5). It was found that the absolute differences between the HB and RM fluxes estimated for a given value of M_n and for r = 50% are generally less than 2.5 W m^{-2}, a significant reduction compared to the fits using (4). The mean differences are 1% or less, 2.5 W m^{-2} over ocean, and −0.1 W m^{-2} over land. The largest contributors to these differences are found at the upper and lower extremes of M_b, which were poorly sampled with the RM data. Thus, the inclusion of humidity in the regressions diminishes the relative differences between the RM and HB data.

Despite the apparent dependence of ΔM on r in Fig. 5, the use of (5) has reduced the RE by only a few tenths of a percent from the nominal case that used (4) and explains only an additional half percent of the variance. This is not surprising, given the large standard deviations found in ΔM for the mean values of r in Fig. 5. Stepwise regression analysis of the data, however, confirms the significance of the relative humidity dependence of the IR–LW relationship. The partial F statistics for M_n ln$r$ over ocean and land are 480 and 200, respectively. Other factors, discussed below, contribute to the REs for each regression.

c. *Sampling and limb darkening*

Temporal differences between the ERBE and GOES data constitute one source of random error in the regression fits. The uncertainty due to time mismatches may be determined by estimating the variation of re-

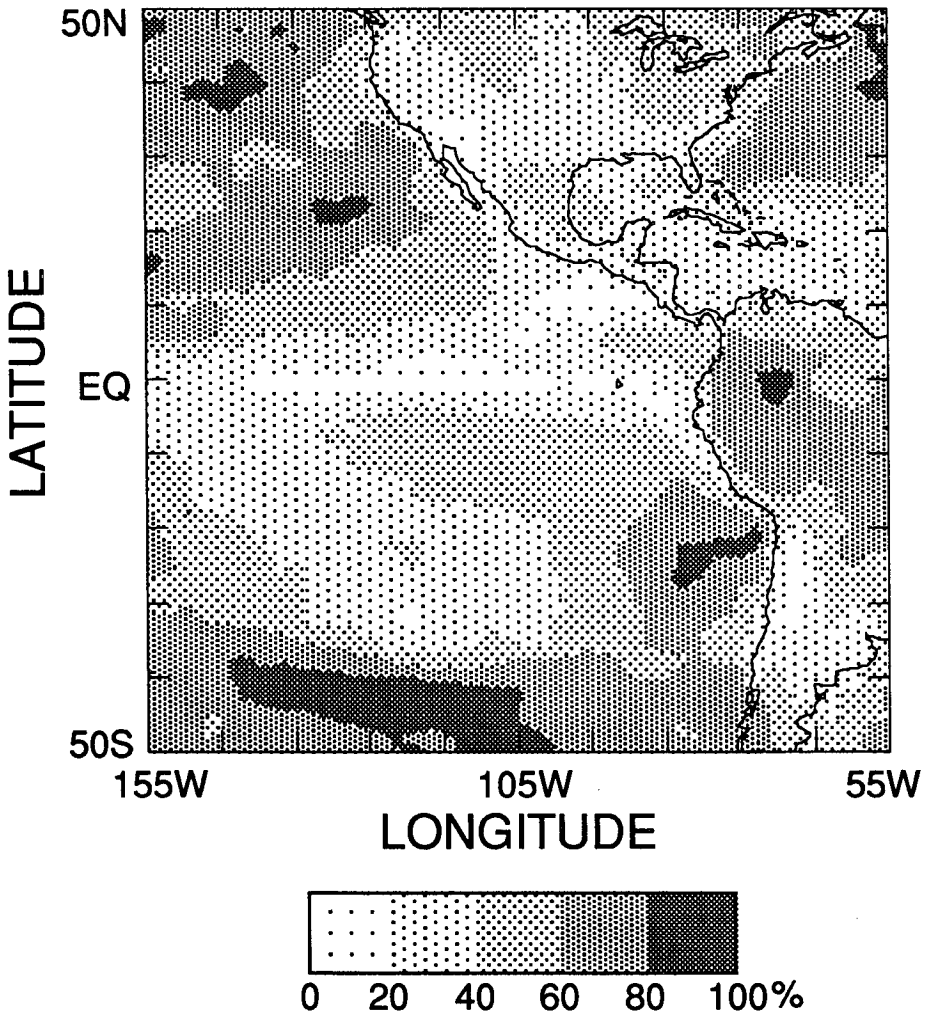

FIG. 4. Mean total cloudiness in percent for HB data, 1–21 April 1985.

gional values of M with time. Applying (4) to the hourly GOES data, it was found that the regional rms hourly changes of M are 5.3 W m^{-2} h^{-1} and 8.2 W m^{-2} h^{-1} over ocean and land regions, respectively. Using the average LW flux for the GOES area of ~245 W m^{-2}, the uncertainties due to the temporal sampling differences are 1.5% and 2.4% over ocean and land regions, respectively, for the HB data using an estimated mean sampling-time difference of 29 minutes. If it is assumed that the random errors from different sources are statistically independent, the values of RE in Table 2 for the HB data can be reduced to only 3.7% and 4.5% over ocean and land, respectively, by removing the temporal sampling differences. Because of the smaller spatial scale, it is more difficult to assess the impact of time sampling on the RM results directly from the GOES data. Ray-matched data from the NOAA-9 will be used to assess the RM time and space uncertainties.

There are also spatial sampling differences in HB dataset. Because of higher resolution, more of the radiance recorded by the GOES pixels actually comes from the assigned region than the fraction of the radiance observed by the ERBE pixels. Assuming a 28-km, nonoverlapping nadir footprint for the ERBS, it is expected that as much as 40% of the pixels lie along the edges of the region. Each edge pixel may have almost half of its footprint in an adjacent region. At $\theta = 70°$, the fraction of edge pixels increases to 62%. For the GOES, the corresponding numbers of "contaminated" pixels are 11% and 14%, respectively. While evaluation of this error is beyond the scope of this paper, its impact may be as great as the temporal sampling differences, especially at higher viewing zenith angles. Another source of random error is the limb-darkening correction applied to normalize and convert the radiances to fluxes. The variation of the ERBE limb-darkening model values with scene type or latitude (Suttles et al. 1989) suggests that the limb-darkening models introduce an uncertainty of no more than 1.5% to the LW–IR relationship.

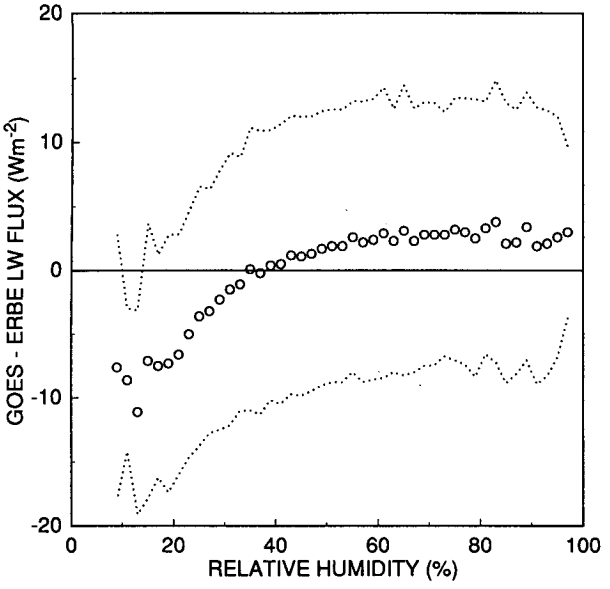

FIG. 5. GOES–ERBE broadband flux differences as a function of relative humidity. Standard deviations shown with dashed curves.

d. *Field-of-view effects*

It was assumed that the nadir ERBS field of view is a 28-km square. The nadir ERBE footprint is actually much larger, however, due to the response characteristics of the scanner. The radiation measured with the ERBE scanner, like most scanning radiometers, comes from an area that is larger than the nominal field of view. As the radiometer scans, the instrument response is recorded at predetermined scan positions. Since the instrument is being irradiated continuously and the sensor requires a finite amount of time to react to a change in signal, the instrument response at a given scan point includes not only the signal from the instantaneous field of view, but also some portion of the signal from the previous field(s) of view. In effect, the field of view along the scan track is smeared. The actual ERBE scanner field of view is also not a square, but rather a clipped diamond. Thus, the actual nadir radiance received by the ERBE scanners is not simply the radiance emanating from a 28-km square on the earth. For example, the nominal footprint for the *NOAA-9* ERBE scanner at a higher altitude is 44 × 65 km (Smith et al. 1986). Slightly more than 94% of the measured radiance, however, comes from an area of 133 × 77 km if one accounts for the instrument response and aperture shape using the instrument point spread function (Whitlock et al. 1989). This instrument response characteristic may be a source of random error in the RM regressions.

To examine this aspect of the analysis, April 1985 and October 1986 data from the ERBE scanner and the AVHRR channels 4 and 5 from the *NOAA-9* satellite were matched and regressed with (4). The *NOAA-9* data were taken during three satellite passes over the central United States and over ocean areas west of Europe, Peru, and Chile. Four regressions were performed, one each using different arrangements of ray-matched AVHRR data to simulate the ERBE footprint. The case comparable to the GOES RM data uses an 8 × 8 array of GAC data. An array of equally weighted 16 × 16 GAC pixels was also used. The other two arrangements convolve the ERBE point-spread function (Whitlock et al. 1989) with the GAC data to account for 24% (8 × 8 array) and 75% (16 × 16 array) of the energy measured with the ERBE scanner. The RE for the 8 × 8 array field of view was 3.9% compared to 3.2% for the 16 × 16 pixel footprint. For the *NOAA-9* LW mean of 242 W m^{-2}, the latter error corresponds to 7.7 W m^{-2}, a value slightly greater than the theoretical uncertainty of 7.0 W m^{-2} for the AVHRR LW computed by Ellingson et al. (1989b). The use of the point spread function did not significantly change these results.

If it is assumed that the AVHRR and GOES IR instruments are comparable and the sampled atmospheric conditions were similar, the total uncertainty in the GOES RM results should be the same (i.e., 7.7 W m^{-2}) as those from the NOAA-9 correlations. The combined land and ocean results in Table 1, however, yield a mean RE of 11.1 W m^{-2}. It is assumed that the difference between the two RE values is due to the combined effects of field-of-view size, temporal differences, and navigation. If the errors contributing to the RE are statistically independent, it may be concluded from the above field-of-view study that the uncertainty in the GOES RM estimates of LW (Table 1) resulting from using a small field of view is $\sqrt{3.9^2 - 3.2^2} = 2.2\%$ or ~5.4 W m^{-2}. The partial error due to spatial and temporal mismatches of the fields of view is, therefore,

TABLE 2. Coefficients and statistics for HB regression fits to Eq. (5).

Background	a_0 (W m^{-2})	a_1	a_2 (W^{-1} m^2)	a_3	R^2	RE [% (W m^{-2})]
Ocean	101.32	3.829	0.0076	−0.2009	0.917	4.0 (10.0)
SE of coefficient (%)	0.7	0.8	5.5	8.7		
Land	78.78	5.168	−0.0132	−0.1947	0.885	5.3 (12.3)
SE of coefficient (%)	0.8	2.4	11.2	7.1		

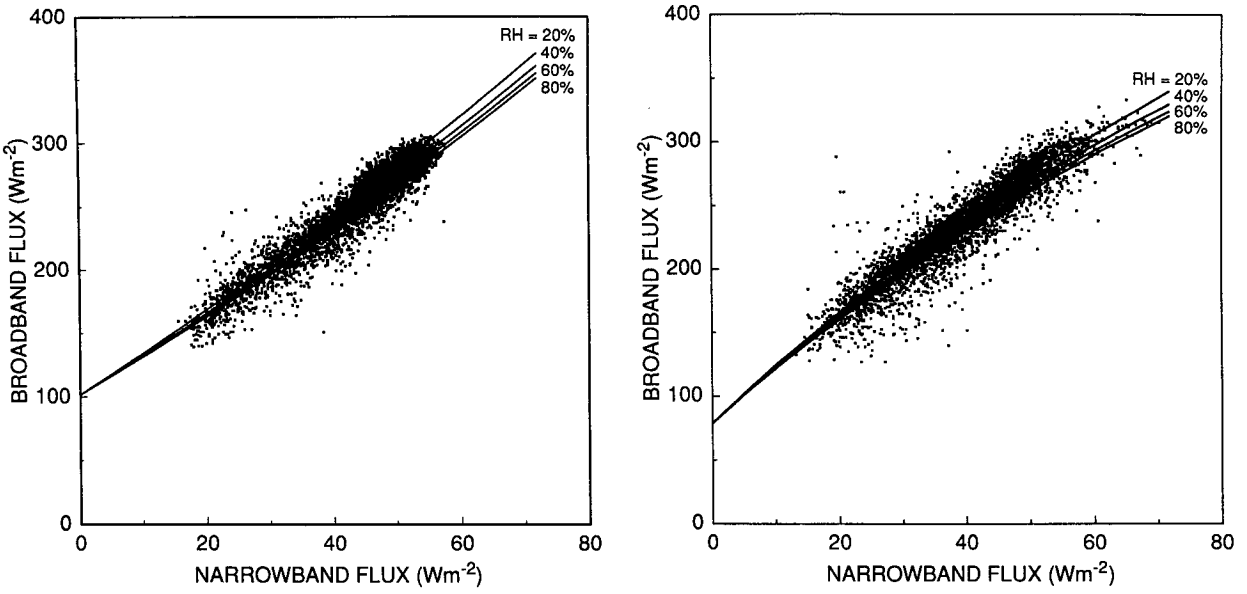

FIG. 6. Correlations using (5) for (a) ocean HB flux data and (b) land HB flux data.

$\sqrt{11.1^2 - 7.7^2 - 5.4^2}$ = 5.9 W m^{-2} or 2.4%. Eliminating these sources of uncertainty would reduce the values of the REs for the ray-matched GOES-ERBE data to approximately 3.2% and 3.7%, respectively, over ocean and land. Accounting for limb-darkening uncertainties (~1.5%) and temporal (~2%) and spatial (~2%) mismatches in the HB data would reduce the HB REs by a similar amount. Since they cover more territory, have a larger range in M_b, and produce the same statistics as the RM data, only HB data will be examined further.

e. *Effects of surface type*

Differences between the land and ocean fits to (5) are minimal except at the extreme values of M_b. Over land, the surfaces can become hotter than the ocean so that larger fluxes (>310 W m^{-2}) are observed. Thunderstorms probably reach very high altitudes over land more often and cover more area than over the ocean. Thus, proportionately more low fluxes (<150 W m^{-2}) are seen over the land areas. With a larger range in the observations, it is likely that the land data provide a better fit at the extremes. The ocean areas provide very good sampling for M_n over the range from 25 to 55 W m^{-2}, however, so that the curve fit up to M_b = 310 W m^{-2} is probably as good as that over land. Yet, the ocean regression yields fluxes that are ~7 W m^{-2} higher than the land results at M_n = 50 W m^{-2}. Application of the coefficient errors in Table 1 to the data in the IR fluxes between 25 and 55 W m^{-2} shows that the two regressions overlap slightly at those flux values, suggesting that there is no statistical significance to the differences in the fits in that range of fluxes. Examination of the standard errors of the means for the data, though, shows that the LW fluxes over ocean at a given value of M_n > 45 W m^{-2} are greater than their land counterparts at the 95% confidence level. This bias may be due to differences in ϵ_s for the IR and LW spectral regions. The surface emissivity over sandy deserts is significantly greater for 10 μm < λ < 12 μm than it is for the entire spectral region between 8 and 14 μm (Prabhakara and Dalu 1976; Sutherland 1986). Over ocean and forests, the surface emissivity is essentially constant. These surface-emissivity spectral dependencies imply that, with all other variables equal, M_b over deserts should be smaller than M_b over oceans or forests for a given M_n. Separate regressions were performed using data from regions classified by ERBE as vegetated land or desert. There were essentially no differences in the resulting curves, indicating that regional variations in surface emissivity are probably not responsible for the differences in the land and ocean regression fits to (5). This apparent lack of surface-emissivity spectral dependency does not necessarily conflict with Prabhakara and Dalu (1976) since their results indicate that the change in ϵ_s from λ = 9 to 11 μm is small over the western hemisphere deserts compared to those in Asia and Africa.

Assuming that the relative effects of CO_2 and relative humidity are the same for both land and ocean, then the only variables in (3) that may explain the land–ocean differences are T_a and T_s. Since water vapor is the most important infrared absorber in the troposphere, the effective atmospheric temperature depends on the combined vertical profiles of temperature and humidity. To account for the variations in these profiles, the effective atmospheric temperature is defined

here as the precipitable-water–weighted temperature of the troposphere above the GOES level. For each HB data point, this parameter was derived from the NMC data by computing the average temperature of each standard layer, multiplying by the precipitable water in the layer, and dividing by the total precipitable water. The resulting values were binned and averaged according to M_n. These means are plotted in Fig. 7 for land and ocean. Despite the lack of data over the ocean for $M_n > 55$ W m^{-2}, it is apparent that there are differences in the results at extreme values of M_n. These differences are shown more clearly in Fig. 8, which reveals that the atmosphere overlying the land scenes is colder for $M_n < 20$ W m^{-2} and for $M_n > 40$ W m^{-2}. These same fluxes correspond approximately to the points of divergence between the land and ocean regression fits to (5). Since T_a is lower over land at the extremes, it follows from (3) that the LW flux over land will be lower than that over ocean at the extremes. Although for a given T_s, M_n will tend to decrease as T_a decreases, the change will probably not be linear with changes in M_b because of the differences in the temperature dependencies of absorption for the H_2O continuum and water vapor lines (Raval and Ramanathan 1989). The reasons for the differences in T_a may be due to the elevations of the radiating surfaces. For example, the greatest values of M_n correspond to clear scenes. Over ocean, the surface radiates from sea level, while over land the mean elevation is closer to 1 km. Thus, for the same atmosphere, the ocean radiates through 1000 mb while the land only radiates through 900 mb with the warmest, usually wettest layer removed. These differences are eliminated for typical cloud scenes but not for deep convective clouds as noted earlier.

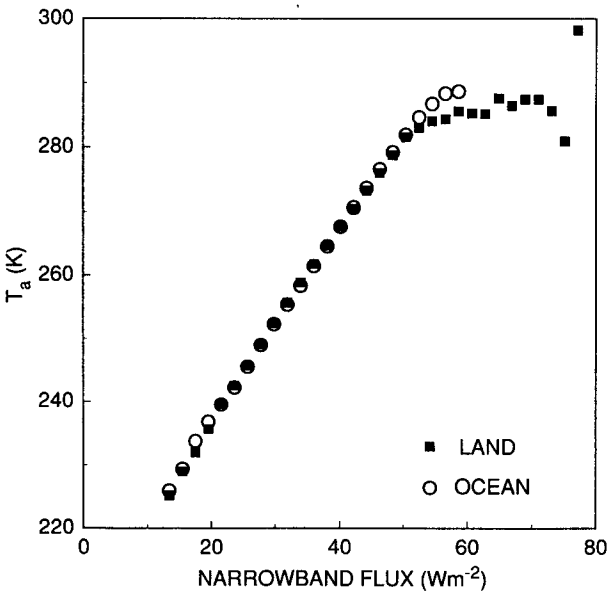

FIG. 7. Variation of T_a with M_n for ocean and land.

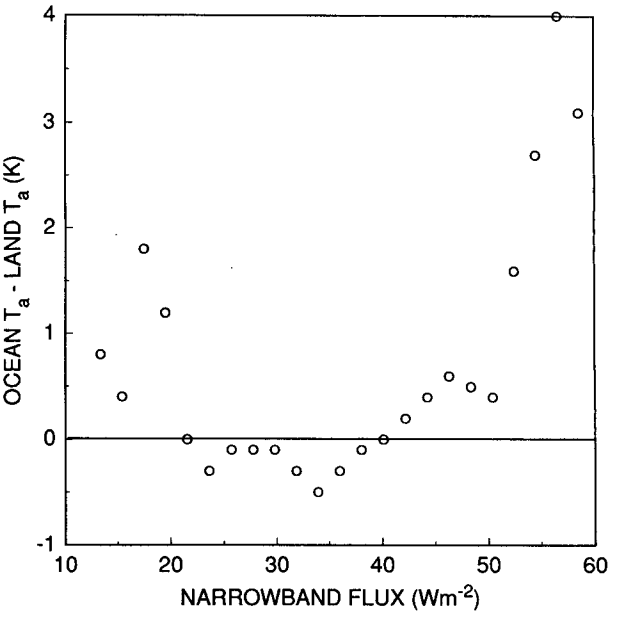

FIG. 8. Difference of mean ocean and land T_a as a function of M_n.

The relationship between surface radiating temperature and the overlying atmosphere may also be a significant source for the disparity between the land and ocean fits. For example, in most situations, the difference between the skin temperature and the near-surface air temperature (e.g., shelter temperature) over oceans is only a few kelvins. During daytime over land, the differences can be much greater as the surface heats more rapidly than the overlying air. This effect results in the temporal lag of a few hours between the skin and air temperatures (e.g., Minnis and Harrison 1984a). Overall, the atmospheric temperature, or T_a, over land does not change much over the course of the day as the surface temperature varies. Except in the case of strong nocturnal surface inversions, the deviation of the skin temperature from the mean lapse rate is most likely to be greater during the day than at night.

This hypothesis was tested by performing the regressions with (4) for night and day data separately. The ocean fits produced values of LW flux during the daytime that were 0.7% higher, on average, than the nighttime values. Analysis of the errors in the resulting coefficients indicated that the differences in the ocean regression curves are not statistically different at the 90% confidence level. The nighttime fit to the land data yielded fluxes that were 2.6% higher than those from the daytime fits. Differences between the coefficients for the day and night land cases are statistically significant at the 95% confidence level. Furthermore, as shown in Fig. 9, the nighttime land fit is almost identical to the average ocean fit. The nocturnal range in M_b is the same as the ocean values. This result supports the conclusion that the thermal "disconnection" of the surface from the atmosphere is the primary driver

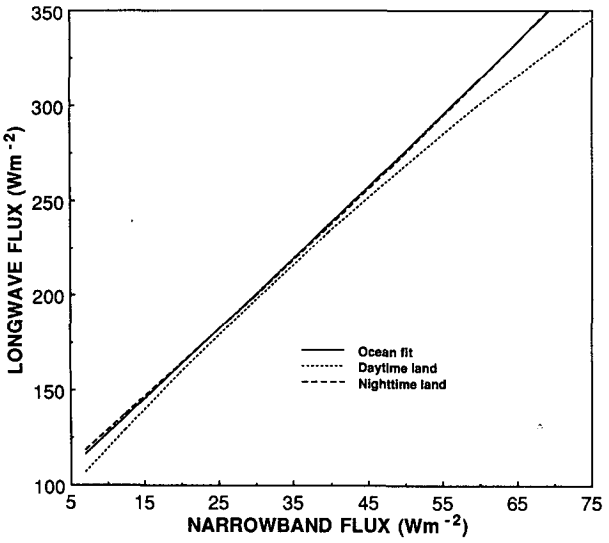

FIG. 9. Comparison of ocean and diurnal land regression fits to (4) for HB data.

of the land–ocean difference. The land regression (Fig. 2b) performed by Minnis and Harrison (1984b) accentuates this difference because all of the data were taken just before noon when the skin–air temperature difference is near its maximum value for clear scenes. For the most part, the differences in T_a at large values of M_n in Fig. 8 may be explained by the diurnal cycle of the surface temperature underneath a relatively constant atmosphere. The slightly greater ocean values of T_a, overall, may be attributed to the elevation effect discussed earlier.

The coefficients for the daytime land regression on (4) are $a_0 = 76.82$, $a_1 = 4.416$, and $a_3 = -0.0104$ with the units given in Table 1. The ocean coefficients given in Table 1 are sufficient to describe the nocturnal land regression fit. While the diurnal differences in the fits to (4) are significant over land areas, use of the single curve in Table 1 is advised to avoid discontinuities between day and night. It falls between the day and night curves for values of M_n between 25 and 50 W m^{-2}. At other values of IR flux, the composite curve follows the daytime fit very closely.

f. Clouds and regional variations

Only about 30% of the rms error in the global fits can be explained by field-of-view, sampling, and limb-darkening differences. The remaining error may be due to variations in the cloud fields and atmosphere. Figures 10a and 10b show the geographical variability of the 21-day mean ERBE HB fluxes and their standard deviations, respectively. Maximum LW flux occurs over the anticyclones and the equatorial clear belt. Minima are found over the Amazon Basin and poleward of 40° latitude. Areas with the greatest variability in M_b correspond to the location of the North American subtropical jet (e.g., Sadler 1975), the Amazon Basin, and the southern Pacific polar frontal zone near 135°W. In the tropics, the regions of maximum variability appear to be collocated with the minima in LW flux. The total cloud cover in Fig. 4 is separated into mean low cloudiness (cloud top lower than 2 km) and mean upper-level (middle plus high, i.e., cloud top higher than 2 km) cloudiness in Figs. 11a and 11b, respectively. Upper-level cloudiness generally includes cirrus clouds. Some very thin cirrus clouds may remain undetected (Minnis et al. 1987). The main areas of low cloud cover correspond to the Pacific anticyclones where very little upper-level cloud cover is found. Higher clouds are common in the areas of the subtropical jet, Amazon rain forest, southern polar front, and the northern storm track near 50°N.

Figure 12a shows the mean differences between all of the HB fluxes and those computed from GOES data using (5). The corresponding standard deviations are given in Fig. 12b. Absolute differences as high as 15 W m^{-2} are found over the southeastern Pacific, over Colombia, and off the western coast of Mexico. The differences are slightly positive over much of the western United States and negative over the eastern United States. The largest positive differences are found over the North American subtropical jet, north of the southern polar front, and over the areas of deep convection in South America. Underestimates of M_b by GOES are most significant over the Pacific off the coasts of California and Chile. The greatest standard deviations (Fig. 12b) occur over the United States–Mexican border, the Amazon Basin, the south-central Pacific, and along the right edge of the domain. Over the first areas, the rapid hourly changes in surface temperature and convective cloud cover maximize the errors due to temporal mismatch. Sparse sampling along the equator and the rapid variations in convective clouds may cause large instantaneous differences over the Amazon. The largest standard deviations in the southern part of the domain appear to be correlated with large variances in LW (Fig. 10b) and decreased sampling due to relatively frequent operational cutoffs of the GOES Southern Hemisphere coverage.

For the entire domain, the rms regional difference is 4.5 W m^{-2}, which is 1.8% of the mean LW flux of 245 W m^{-2}. The mean regional difference is nonzero, 0.3 W m^{-2}, because of unequal sampling of the regions. Use of (4) results in an rms error of 5.0 W m^{-2} with a range of −20 to 15 W m^{-2}. Thus, the inclusion of relative humidity decreases the regional bias errors by 10%. GOES underestimates M_b over marine areas having the lowest relative humidities. This indicates that the RH term in the regression fits (Table 2) cannot fully account for the differences between the atmosphere over these areas and the average atmosphere implied in the coefficients. These same areas have abundant low-level clouds (Fig. 11a). The areas where GOES overestimates the flux have no particular relative

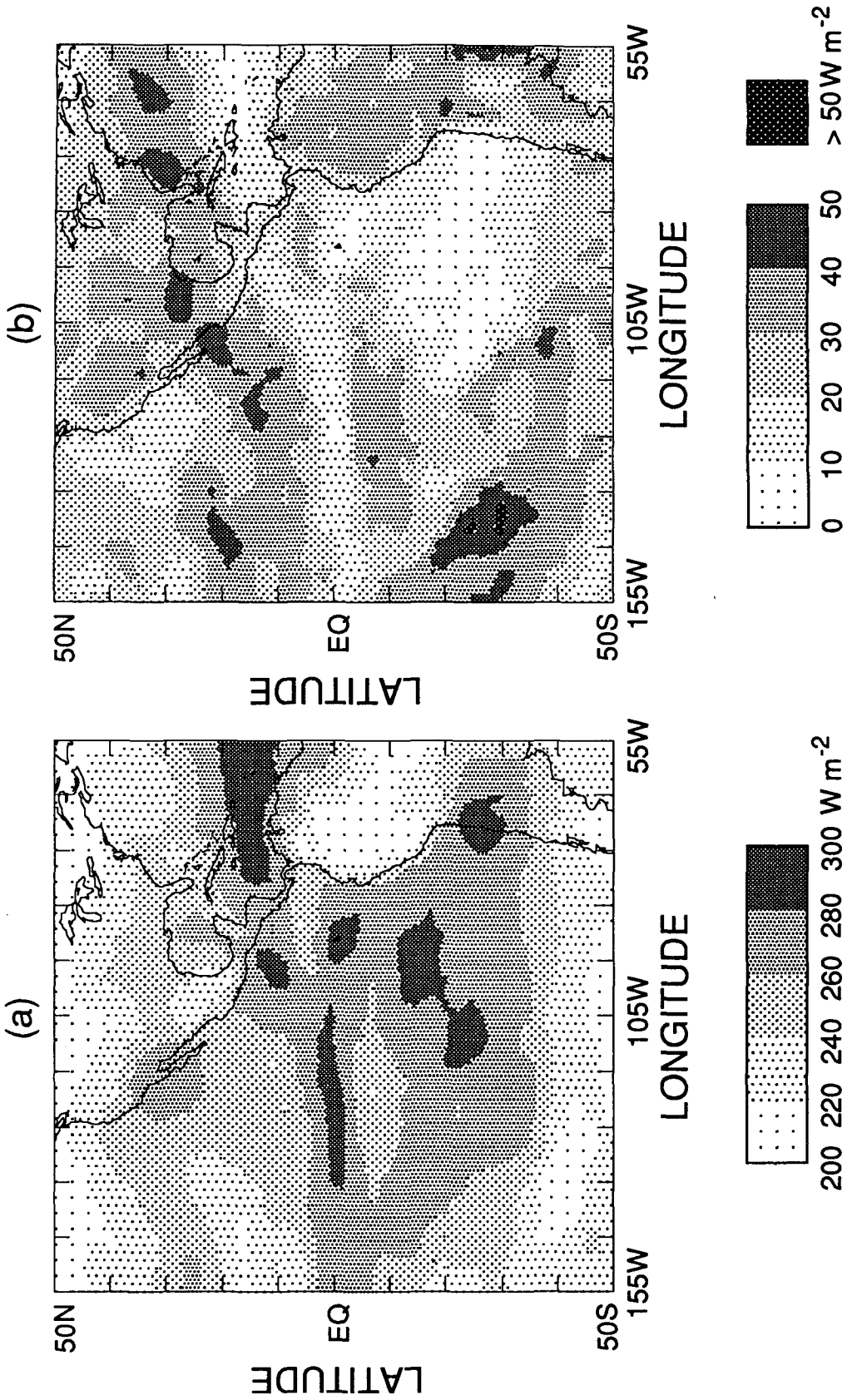

FIG. 10. Regional means of ERBE (a) HB fluxes and (b) their associated standard deviations.

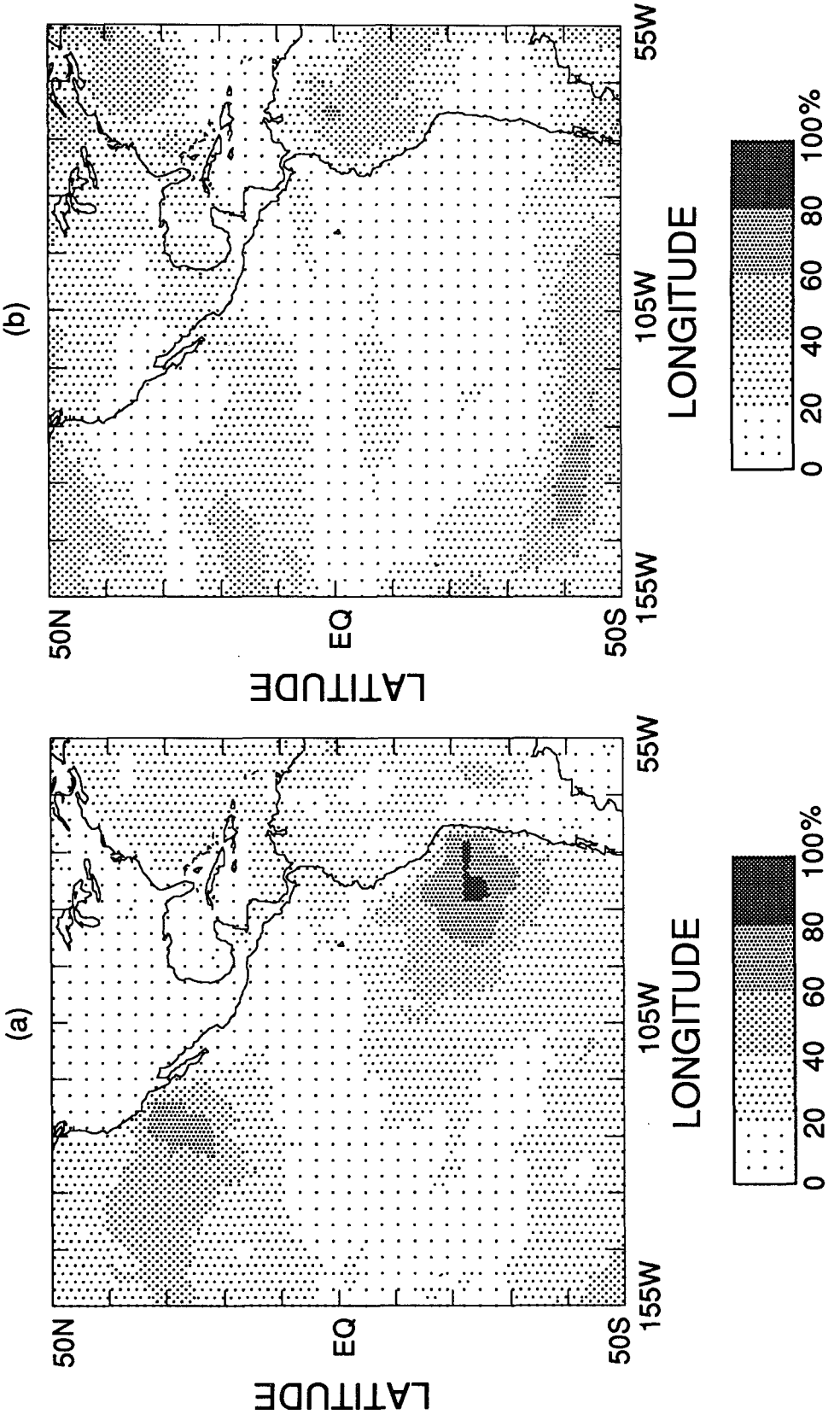

FIG. 11. Regional mean (a) low cloudiness and (b) upper-level cloudiness in percent, 1–21 April 1985.

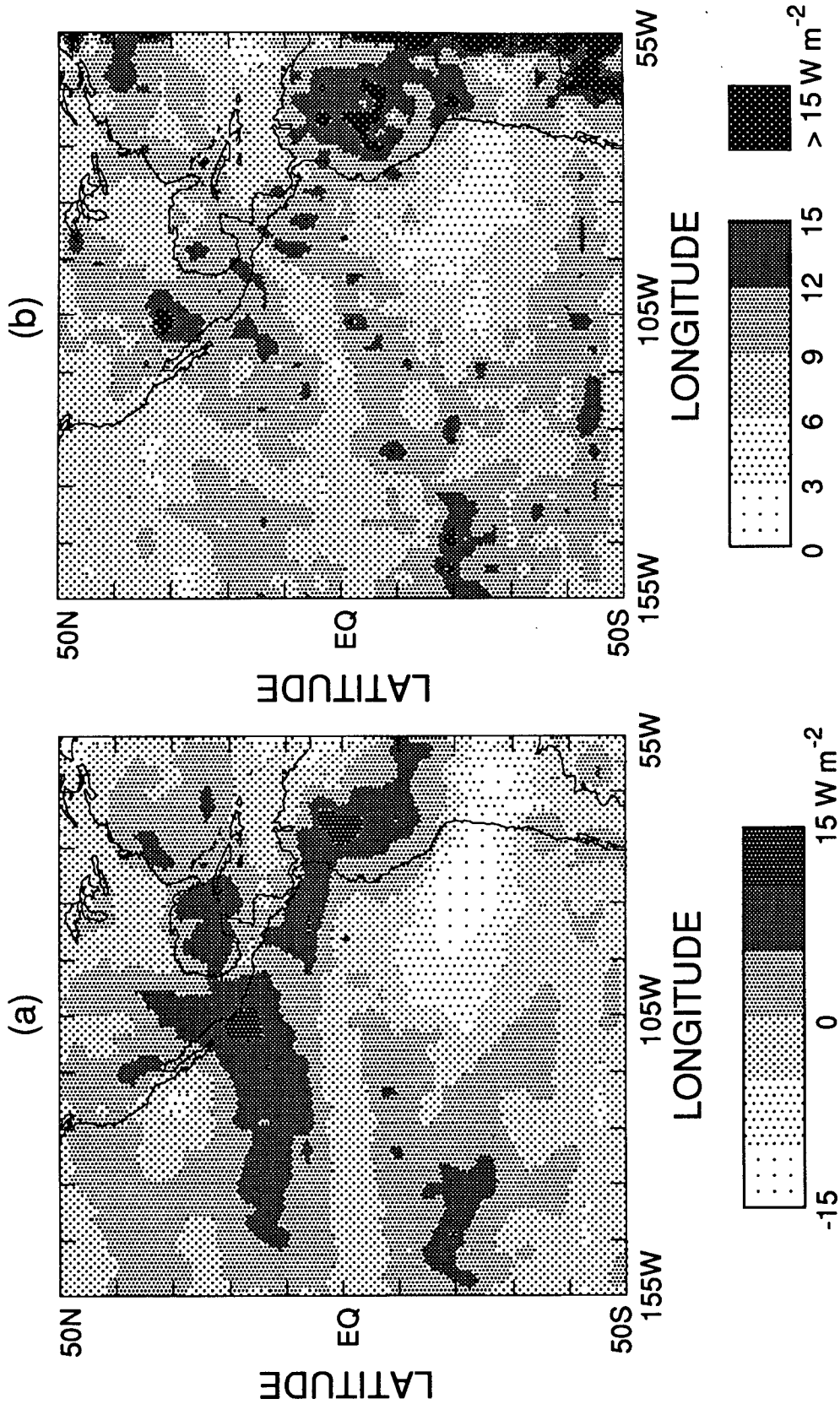

FIG. 12. Regional (a) means and (b) standard deviations of the differences between ERBE fluxes and GOES fluxes computed with (5) using HB data.

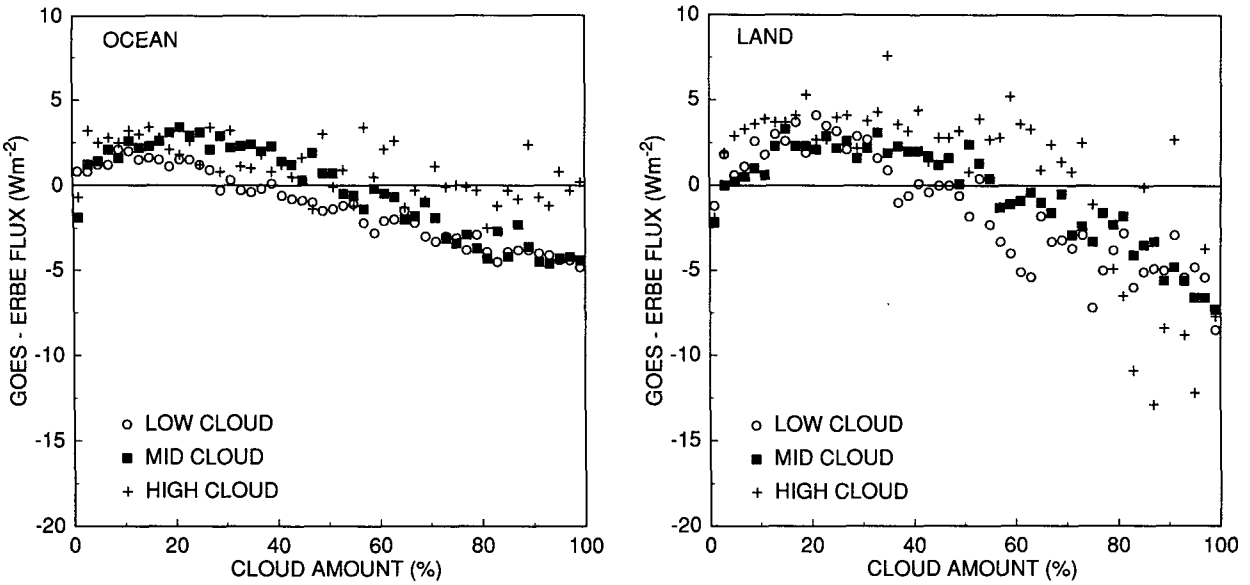

FIG. 13. GOES–ERBE broadband flux difference as a function of cloudiness for (a) ocean and (b) land using (5).

humidity feature. They do, however, have substantial upper-level cloudiness, which generally indicates that cirrus clouds are present as well.

To examine the relationship between the flux differences and cloud type, values of ΔM resulting from (5) were binned and averaged according to the fraction of each type of cloud cover. The resulting means are shown in Figs. 13a and 13b for ocean and land, respectively. Although the trends are the same for both surfaces, the variations over land are much noisier. Increasing low clouds leads to underestimates by GOES, while the presence of high clouds, on average, corresponds to a GOES overestimate of the flux. Midlevel cloud amounts less than 50% are associated with overestimates by GOES. Larger amounts of midlevel cloudiness are apparently related to GOES underestimates.

These results are similar to the theoretical calculations of Ellingson and Ferraro (1983, see their Fig. 7). For example, Fig. 14 compares their theoretical results for a global LW–IR regression applied to cirrus clouds between 450 and 350 mb with the present results for high clouds over all surfaces. The observations are noisy but have the same trends and magnitudes as the computations. Ellingson and Ferraro (1983) also found considerable scatter in their results from one sounding to the next. The Ellingson and Ferraro (1983) differences for midlevel clouds range from ~ 1.5 W m^{-2} for no cloud cover, to zero at 50% cloudiness, and to nearly -3 W m^{-2} at 100% cloud cover. The greatest discrepancies between the Ellingson and Ferraro (1983) and current results are found for low clouds. The mean differences in the theoretical data vary slowly from -2 to -3 W m^{-2}. Their counterparts in Fig. 14 range from about 2 W m^{-2} to approximately -5 W m^{-2}. Nonetheless, the overall trends are the same. On average, both theoretical and empirical differences are most positive for high clouds and most negative for low clouds. There is virtual agreement in the differences for all cloud levels in both datasets at cloud amounts of 100%.

This level of agreement between the satellite and computed LW–IR differences is remarkable given the room for disagreement. The theoretical calculations used a sample of 96 soundings taken mostly over Northern Hemisphere land. The 45 cloudy soundings apparently contained only one level of clouds. A quadratic fit in effective blackbody temperature was used in the theoretical study. On the other hand, a majority of the satellite data was taken over ocean areas. The low clouds over ocean generally occur under a strong inversion, which is probably infrequent or absent in the cloudy soundings. No polar regions or major deserts

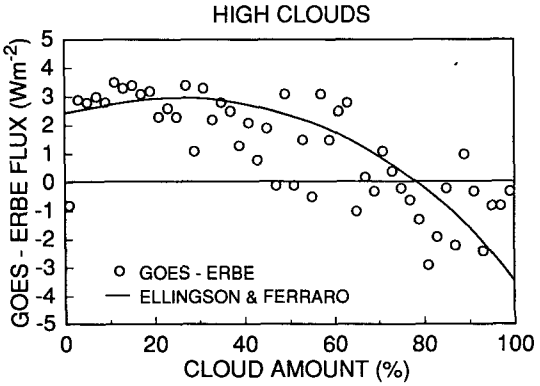

FIG. 14. Comparison of theoretical and empirical flux differences for global regression fits applied to scenes with high clouds.

fall in the GOES domain. Mixed-level clouds are common in the satellite dataset. Thus, the empirical results, especially at small cloud amounts, are not necessarily representative for pure single-layer clouds. The empirical regression also contains the relative humidity term, which is absent in the Ellingson and Ferraro (1983) fit. This extra term, because it only uses moisture above the effective cloud level, already implicitly contains some information about cloud level. Its impact on the relationship is minor, however. Despite these sources for disagreement, the common trends support the conclusion that cloud height is a significant factor in the LW–IR relationship.

Layer cloud amounts are included in the relationship between M_n and M_b in the form:

$$M_b = a_0 + a_1 M_n + a_2 M_n \ln r + a_3 C_1 + a_4 C_2, \quad (6)$$

where C_1 and C_2 are the low- and upper-level cloud fractions, respectively. The coefficients and their standard errors are listed in Table 3. Inclusion of cloud data in the relationship has only reduced the RE by an additional 0.1% and explained an additional 0.2% of the variance. This small decrease is not surprising given the uncertainties resulting from the natural variability of atmospheric structure (e.g., Ellingson and Ferraro 1983). Stepwise regression analysis indicates that the low-cloud term is statistically significant at the 95% confidence level for ocean. The upper-level cloud term is not significant at that confidence level over ocean. In contrast, over land the high-cloud term is clearly significant, while the low-cloud coefficient is only marginally significant. The mean regional differences are plotted in Fig. 15. Despite the negligible decrease in the RE, the areas within the ± 10–15 W m^{-2} contours have noticeably decreased. The standard deviations of the differences (not shown) are essentially unchanged from those in Fig. 12b. Overall, however, the rms regional mean differences are 4.1 W m^{-2} or 1.7% and large errors are still found in some regions. Use of the cloud data to evaluate M_b from M_n has only reduced the regional error by 9% relative to the simple humidity fit.

How cloud cover affects this relationship is a relatively complex matter. Discussion of the cloud-cover effect may be simplified somewhat by considering (3) and keeping in mind the earlier discussion of the differences in the regressions over land and water. The altitude of the cloud cover and, therefore, the radiating surface affects the values of T_a and ϵ_a. Both atmospheric emissivity and effective atmospheric temperature will vary differently with altitude for the LW and IR because of variations in both water vapor and carbon dioxide. The optical depth of CO_2, which does not affect the IR, is directly proportional to the pressure thickness of the atmosphere. Increasing the altitude of the cloud or the surface decreases the pressure thickness and the values of T_a and ϵ_a only for the LW transmission. Increasing the altitude of a surface implies a colder surface radiating temperature. Since the proportion of total water vapor emission due to the continuum varies with surface radiating temperature (e.g., Raval and Ramanathan 1989), there will be differences in the relationship between LW and IR over surfaces of different altitude due to water vapor. Combining both water vapor and carbon dioxide leads to the conclusion that, for a global fit, T_a over low clouds will be greater than the mean value implied in the global fit. Similarly, T_a will be smaller for high clouds than for the mean of the global fit. Thus, in areas predominated by one cloud type, the average radiating temperature will correspond to that cloud type resulting in an under- or overestimate of M_b. It is not just coincidence that the mean error in the GOES-derived LW flux is near zero for 50% midlevel cloud cover. Midlevel cloudiness probably corresponds to the mean conditions for the regressions.

A regression was performed including a term proportional to $T_a \ln r$, but no improvement was gained relative to using (4). Some of the lack of improvement may be due to large uncertainties in the vertical profiles of temperature and humidity over remote areas. This aspect was examined by regressing only on data from those land regions between 30° and 50°N, where a dense rawinsonde network provides soundings for the NMC analyses. It is assumed that the vertical profiles are substantially more accurate over the United States than anywhere else in the domain. In the United States case, the amount of explained variance increased by 0.8% by using (5) instead of (4). This increase is twice that found for all land areas. Part of the low performance of the relative humidity term may also be due to the inability of the NMC analyses to resolve strong inversions such as those over marine stratocumulus.

TABLE 3. Coefficients and statistics for regression fits of HB data to Eq. (6.

Background	a_0 (W m^{-2})	a_1	a_2	a_3	a_4	R^2	RE [% (W m^{-2})]
Ocean	93.86	4.186	−0.1626	0.0487	−0.0267	0.919	3.9 (9.8)
SE of coefficient (%)	2.1	1.3	5.6	11.4	40.1		
Land	113.12	3.821	−0.1979	0.0456	−0.1046	0.887	5.2 (12.1)
SE of coefficient (%)	1.3	1.3	6.9	17.8	8.3		

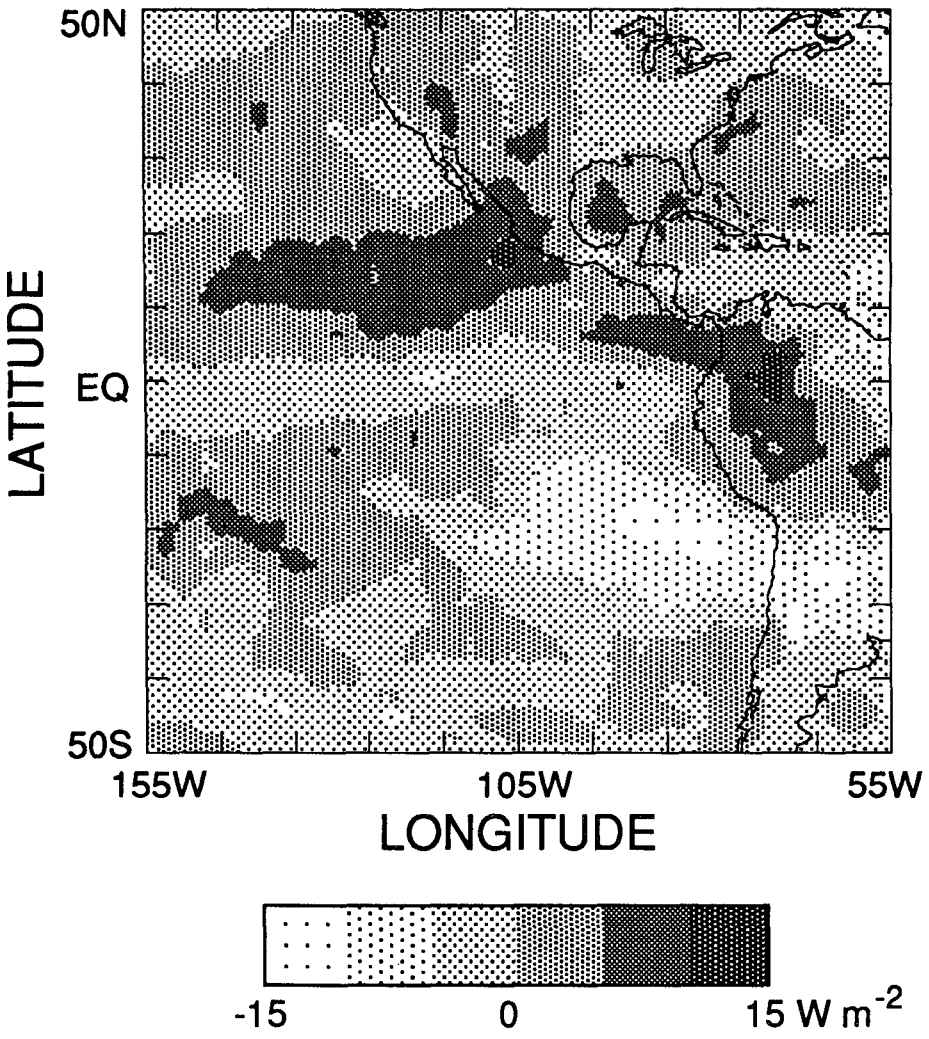

FIG. 15. Same as Fig. 12a except GOES flux computed using (6).

For example, Minnis et al. (1990) showed a comparison of mean July 1987 aircraft and NMC analyses of the vertical profiles of temperature and humidity over the Pacific off the California coast in a region of marine stratocumulus. In that limited comparison, the strong boundary-layer inversion at cloud top was absent in the NMC data and the specific humidity between cloud top (~920 mb) and 850 mb was overestimated by more than 200%. The cloud-top temperature was the same as the NMC temperature interpolated to 680 mb. These examples suggest that the effects of T_a and r on the narrowband–broadband flux relationship may be better understood with a dataset that is more accurate and highly resolved than the NMC analyses.

The presence of a strong inversion may, by itself, produce a substantial impact on the IR–LW relationship. For example, a very dry, thick inversion over a marine stratocumulus deck will have little effect on the upwelling IR radiance because of the lack of water vapor in the overlying air. The cloud-top temperature may be as much as 12 K colder than the overlying air (e.g., Neiburger et al. 1961) over marine stratocumulus, yet the effective IR blackbody temperature observed with the satellite is very close to the actual cloud-top temperature. Inversions run counter to the implicit mean atmospheric structure of decreasing temperature with increasing altitude so that areas with persistent inversions have a value of T_a, which deviates significantly from the global mean. This inversion effect is opposite that seen for the warm, daytime land surface.

Another effect on this relationship that may be more directly tied to cloud cover is the dependence of cloud emissivity on wavelength and phase. It has been shown that the absorption efficiency of small droplets is much smaller for $\lambda < 10$ μm than it is at longer wavelengths (Ackerman and Smith 1990). Thus, compared to the average cloud, the cloud containing small water droplets will absorb less radiation at shorter wavelengths so

that more radiation from lower levels will pass through the cloud. Therefore, the effective radiating temperature for all wavelengths will be greater than that for the IR region alone. This mechanism may play a minor role in the overestimates of LW over regions of stratocumulus clouds. The cloud emissivity also depends on phase. Theoretical calculations for ice clouds reveal that the emissivity will vary with particle size and wavelength (Ackerman and Smith 1990). Thus, over regions with persistent cirrus clouds (e.g., subtropical jets) there may be a shift of the effective cloud radiating temperature because of these microphysical effects. Furthermore, the peak of the Planck function for low clouds will generally be less than 11 μm. For high clouds, the peak occurs for $\lambda > 12$ μm. The relative influence of the microphysical effects will also be affected by the shift in the peak energy with altitude. Considering these microphysical factors and the radiating temperature of the atmosphere, it is not surprising that simple insertion of low- or upper-level cloud amount into the equation has only a minor effect.

g. *Regional fits*

The instantaneous rms errors in the LW fluxes derived with the global fits may be tolerable when long-term averages are considered. The mean regional errors presented in Figs. 12a and 15, however, show quite clearly that global fits—even those distinguishing land from ocean—do not provide the broadband flux accuracy required for long-term monitoring of outgoing longwave radiation. One approach to minimizing the regional bias errors is to obtain a fit to the model for each region. Regional coefficients were derived for (5) using all of the HB data for each region. The fits were quite successful in reducing the mean regional flux error to 0.1% with an rms of 0.5%. The standard deviations of the instantaneous regional errors are still significant, having a mean value of 3.2% or 7.7 W m^{-2}. This value is only 2.3 W m^{-2} greater than the standard deviation in a ray-matched intercalibration of the *NOAA-9* and ERBE LW scanners. Thus, the regional fits provide data that are almost as well calibrated as the ERBE instruments are to each other.

Direct substitution of the narrowband fluxes for the ERBE fluxes in the ERBE time–space averaging algorithm provides a more accurate measure of the capability of using GOES IR data for estimating the uncertainties in the regional ERBE monthly mean LW fluxes due to sampling and averaging. The HB GOES data were converted to instantaneous LW fluxes with the global and regional fits to (5) and used in the ERBE time–space averaging algorithms (Brooks et al. 1986) as if they were ERBE fluxes. The resulting averages were then compared to the corresponding 21-day means derived from the measured ERBE fluxes. On average, the ERBE regional means simulated with the GOES data converted with the global fits were 0.2 ± 4.3 W m^{-2} greater than those computed from the ERBE data. Regional 21-day means derived with the regional regression fits are within 0.0 ± 1.5 W m^{-2} or 0.6% of those computed with the ERBE data.

While it is evident that regional regression fits are satisfactory for deriving datasets that can be used effectively for validation, it is unlikely that such an approach could ever substitute for direct measurement of the broadband LW flux. In this study, the availability of simultaneous LW measurements allows a regional calculation of the regression coefficients. Long-term monitoring of the outgoing LW using IR data without the benefit of coincident LW measurements is a different matter. As the weather or climate changes over a given area, so will the regression coefficients. Thus, regional regression coefficients derived at any given time will not necessarily be valid at some other time. Attempts to use independent variables such as humidity and cloud cover as a measure of weather or climate change in a global regression were inadequate. These partially successful efforts to improve the global regressions do not imply that further improvements are impossible. More accurate global regressions may be derived if better, more highly resolved auxiliary data, i.e., atmospheric profiles of temperature and humidity, were available.

4. Conclusions

The effects of sampling, relative humidity, surface type, cloud cover, and atmospheric temperature on the relationship between narrowband IR flux and broadband LW flux have been examined here. Regression fits of IR and LW radiances using a relatively large dataset that is spatially, but not temporally, well matched (HB data) are statistically as good as, or better than, relatively small datasets that are well matched in time, space, and direction (RM data). Furthermore, the former dataset is much easier to obtain than the latter. It has been concluded that global fits using the measured narrowband flux with coincident measurements of atmospheric relative humidity and cloud cover produce more reliable values of broadband flux than fits that use only the measured broadband flux. The fits should be performed for various earth surface backgrounds. The resulting regional rms error in the monthly mean outgoing longwave flux using the best set of regression coefficients is 1.7%. Although this implies that a fairly acceptable LW flux may be derived from the GOES, especially in light of its sampling capabilities, it is important to realize that the errors are not randomly distributed over the domain. They tend to be concentrated over particular geographic locations with systematic errors as large as 15 W m^{-2}. Attempts to remove these regional biases with available auxiliary data have been only minimally successful.

By using individual regional regressions, it possible to essentially eliminate bias errors in the monthly mean

LW flux derived from narrowband data. Such regional regressions will be useful for time–space averaging validation of experimental broadband measurement projects such as ERBE. Furthermore, the regional regressions will permit operational IR data to be used more accurately in other efforts requiring estimates of the outgoing longwave flux at high temporal and spatial resolution. Since long-term variations in the outgoing longwave flux due to climate changes may be relatively small, it is concluded that it is necessary to measure the outgoing flux over the entire spectrum to unambiguously detect any trends. For example, a change in both atmospheric humidity and surface temperature may produce a change in the IR flux but not cause a significant change in the outgoing LW irradiance. Further significant improvements in our understanding of the narrowband-to-broadband flux relationship are required before the single-channel narrowband data will be sufficient for monitoring longwave flux variations. Those improvements, if possible, await further research into the interactions of thermal radiation, clouds, the atmosphere, and the surface and the development of more accurate temperature and humidity soundings of the atmosphere.

Acknowledgments. We gratefully acknowledge the assistance of Sherri Morgan and Sarah Eckhause of Computer Sciences Corporation in the reduction of the large volumes of GOES data. The dedicated efforts of David R. Doelling in the cloud analysis and by Patrick W. Heck in the AVHRR analyses are deeply appreciated. Both researchers are from the Lockheed Engineering and Sciences Company. Software developed by Lockheed's Dr. Shashi Gupta was used for matching the AVHRR and ERBE data. Comments by the reviewers of the original manuscript are appreciated.

REFERENCES

Ackerman, S. A., and W. L. Smith, 1990: IR spectral characteristics of cirrus clouds. FIRE Science Results—1989. NASA CP-3079, 441–446.

Barkstrom, B. R., 1984: The Earth Radiation Budget Experiment (ERBE). *Bull. Amer. Meteor. Soc.*, **65,** 1170–1185.

Brooks, D. R., and P. Minnis, 1984: Simulations of the earth's monthly regional radiation balance derived from satellite measurements. *J. Climate Appl. Meteor.*, **23,** 155–160.

——, E. F. Harrison, P. Minnis, J. T. Suttles and R. S. Kandel, 1986: Development of algorithms for understanding the temporal variability of the earth's radiation balance. *Rev. Geophys.*, **24,** 422–438.

Draper, N., and H. Smith, 1981: *Applied Regression Analysis. 2nd ed.*, John Wiley & Sons, 709 pp.

Ellingson, R. G., and R. R. Ferraro, 1983: An examination of a technique for estimating the longwave radiation budget from satellite radiance observations. *J. Climate Appl. Meteor.*, **22,** 1416–1423.

——, D. J. Yanuck and A. Gruber, 1989a: Effects of the choice of meteorological data on a radiation model simulation of the NOAA technique for estimating outgoing longwave radiation from satellite observations. *J. Climate,* **2,** 761–765.

——, ——, H.-T. Lee and A. Gruber, 1989b: A technique for estimating outgoing longwave radiation from HIRS radiance observations. *J. Atmos. Oceanic Techol.*, **6,** 706–711.

Gruber, A., and J. S. Winston, 1978: Earth-atmosphere radiation heating based on NOAA scanning radiometer measurements. *Bull. Amer. Meteor. Soc.*, **59,** 1570–1573.

Harrison, E. F., P. Minnis and G. G. Gibson, 1983: Orbital and cloud cover sampling analyses for multisatellite earth radiation budget experiments. *J. Spacecr. Rockets,* **20,** 491–495.

Menzel, P., 1980: Prelaunch study of VAS-D performance. Contract Report (NAS5-21965), [Available from the author at the University of Wisconsin Space Science and Engineering Center, Madison, WI 53706.]

Minnis, P., and E. F. Harrison, 1984a: Diurnal variability of regional cloud and clear-sky radiative parameters derived from GOES data. Part I: Analysis method. *J. Climate Appl. Meteor.*, **23,** 993–1011.

——, and E. F. Harrison, 1984b: Diurnal variability of regional cloud and clear-sky radiative parameters derived from GOES data. Part III: November 1978 radiative parameters. *J. Climate Appl. Meteor.*, **23,** 1032–1051.

——, ——, and G. G. Gibson, 1987: Cloud cover over the equatorial eastern Pacific derived from July 1983 ISCCP data using a hybrid bispectral threshold method. *J. Geophys. Res.*, **92,** 4051–4073.

——, P. W. Heck, D. F. Young, C. W. Fairall and J. B. Snider, 1990: Comparison of stratocumulus cloud properties from simultaneous satellite and surface-based instrumentation. *AMS Conf on Cloud Physics,* San Francisco, Amer. Meteor. Soc., 161–166.

Montogomery, H. E., and L. W. Uccellini, 1985: VAS demonstration: (VISSR Atmospheric Sounder) description and final report. NASA RP 1151, 170 pp. [NTIS 86N-13867.]

Nieburger, M., D. S. Johnson and C. W. Chien, 1961: Studies of the structure of the atmosphere over the eastern Pacific Ocean: The inversion over the eastern Pacific Ocean. *Univ. Calif., Berkeley, Publ. Meteor.*, **1,** 1–94.

Ohring, G., A. Gruber and R. G. Ellingson, 1984: Satellite determination of the relationship between total longwave radiation flux and infrared window radiance. *J. Climate Appl. Meteor.*, **23,** 416–425.

Prabhakara, C., and G. Dalu, 1976: Remote sensing of the surface emissivity at 9 μm over the globe. *J. Geophys. Res.*, **81,** 3719–3724.

Raval, A., and V. Ramanathan, 1989: Observational determination of the greenhouse effect. *Nature,* **342,** 758–761.

Sadler, J. C., 1975: The upper tropospheric circulation over the global tropics. University of Hawaii Tech. Rep. UHMET-76-05, 35 pp.

Smith, G. L., R. N. Green, E. Raschke, L. M. Avis, J. T. Suttles, B. A. Wielicki and R. Davies, 1986: Inversion methods for satellite studies of the earth's radiation budget: Development of algorithms for the ERBE mission. *Rev. Geophys.*, **24,** 407–421.

Sutherland, R. A., 1986: Broadband and spectral emissivities (2–18 μm) of some natural soils and vegetation. *J. Atmos. Oceanic Technol.*, **3,** 199–202.

Suttles, J. T., R. N. Green, G. L. Smith, B. A. Wielicki, I. J. Walker, V. R. Taylor and L. L. Stowe, 1989: Angular radiation models for earth-atmosphere system, Volume II—longwave radiation. NASA RP-1184, Vol. II, 84 pp. [NTIS 89N20587.]

WCRP, 1987: International Satellite Cloud Climatology Project (ISCCP) description of reduced data. World Climate Research Programme WMO/TD-No. 58, 143 pp. [Available from Dr. William B. Rossow at NASA Goddard Space Flight Center Institute for Space Studies, 2880 Broadway, New York, NY, 10025.]

Whitlock, C. H., L. H. Hoffman and R. F. Arduini, 1989: ERBE/NOAA-9 observations for the FIRE/SRB Wisconsin experiment region from October 14 through October 31, 1986. NASA TM-101627, 31 pp. [NTIS 89N26328.]